Title

INVESTIGATIONS OP HEAT TREATMENTS FOR IMPROVED PROPERTIES OF LOW CARBON Fe-0.l2%C-0.5%Mn STEELS

Author

Koo, Ja-Young.

Publication Date

1975-02-01

LBL-3587
c.1

INVESTIGATIONS OF HEAT TREATMENTS FOR IMPROVED PROPERTIES OF LOW CARBON Fe-0.12%C-0.5%Mn STEELS

Ja-Young Koo
(M.S. thesis)

February 1975

Prepared for the U. S. Atomic Energy Commission
under Contract W-7405-ENG-48

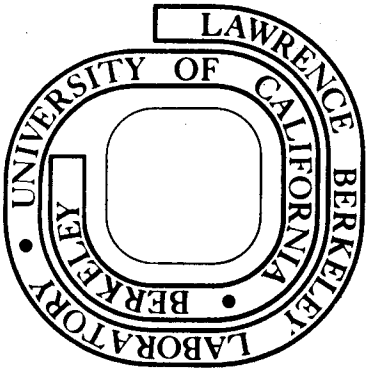

LBL-3587
c.1

DISCLAIMER

INVESTIGATIONS OF HEAT TREATMENTS FOR IMPROVED PROPERTIES OF LOW CARBON Fe-0.12%C-0.5%Mn STEELS

Contents

INVESTIGATIONS OF HEAT TREATMENTS FOR IMPROVED PROPERTIES OF LOW CARBON Fe-0.12%C-0.5% Mn STEELS

Ja-Young Koo

Inorganic Materials Research Division, Lawrence Berkeley Laboratory and Department of Materials Science and Engineering, College of Engineering; University of California, Berkeley, California 94720

ABSTRACT

A new non-standard heat-treating process has been investigated with the aim of improving the mechanical properties of low carbon Fe - 0.12%C - 0.5% Mn steels. The process consists of alternate thermal cycling in the γ range and two phase ($\alpha + \gamma$) range with intermediate iced brine quenching. Microstructures, consisting of variable amounts of martensite, proeutectoid ferrite and retained austenite were produced. These were characterized using optical and transmission electron microscopy.

The tensile properties resulting from the heat treatment were compared with those from conventional and rapid heat treatment methods. The factors leading to superior combinations of yield strength and elongation ductility are thought to be amount of martensite, dislocation substructure, grain size, and retained austenite.

I. INTRODUCTION

A great deal of work has been carried out to increase toughness and strength of medium and high carbon alloy steels[1-3] while comparatively little emphasis has been directed towards a fuller understanding of the ductility and strength of low carbon steel, particularly plain-low carbon steels.

It appears that there is considerable scope for exploiting the potential ductility of plain-low carbon steel with adequate strength. In steels containing ferrite and pearlite the increase in strength found by increasing carbon is very effective,[4] but there are major disadvantages associated with this increase, namely, inadequate ductility and weldability.[5] For a given composition of ferritic and pearlitic steel, it has been shown that the most important factor controlling strength and associated ductility is grain size.[5,6] Following the work of Grange,[7] a rapid heat treatment process was developed. This consisted of repeated cycles of rapid austenitizing and cooling and has now become a practical method to achieve ultrafine grain size. However, the increase in strength due to ultrafine grain size in steels with a mixture of ferrite and pearlite is not sufficient to reach the required strength level in some engineering applications, e.g. transportation in which achievement of weight reduction is an urgent task for design engineers.

If a plain-low carbon steel, subjected to thermal cycling to obtain fine grain size by conventional or rapid heat treatment technique, is quenched to form martensite, using a standard quenching medium for the purpose of increasing strength, ductility drops

drastically and undesirable microstructures result due to low hardenability. Appreciable savings in weight and cost can be obtained if the ductility, with adequate strength, in a low carbon steel can be utilized.

The use of the ($\alpha + \gamma$) two phase field for improving mechanical properties of steels has been recognized by other investigators as in the maraging steels by Jin,[8] and the low alloy steels by Snape and Church.[9] However, the transformation behavior and the beneficial effect resulting from using two phase decomposition are dissimilar in different systems[5] and conditions.

The aim of this work is to extend the thermal cycling techniques to simple, low carbon steels, by manipulating variables such as grain size and transformation substructures, so as to improve ductility at desirable strength levels without using mechanical or thermo-mechanical treatments.

II. EXPERIMENTAL PROCEDURE

A. Materials and Initial Heat Treatment

The materials used in this investigation were commercial automobile structural steels (INNA) and 1010 steel whose alloy compositions are given in Table 1. The steel alloys, hereforth denoted "A" and "B" respectively, were donated by General Motors Research Laboratories, courtesy of Dr. G. W. Bailey.

"A" steel was received in the form of 1/8in. pieces of rolled sheet in the nitrogenized and spheroidized condition. "B" steel was received as 1/8in. hot rolled sheet. Tensile and transmission electron microscopy specimens were prepared by cutting the sheets into slightly bigger dimensions than the exact tensile specimens, homogenized under an argon atomosphere at 1100°C for two hours, and then furnace cooled. The specimens were austenitized in an argon atmosphere at 1100°C for 30 minutes and then quenched directly into agitated iced brine. Later transmission electron microscopic examination showed that the as-quenched specimens were free of undissolved carbides and were almost completely martensitic. Chemical analysis was done for several elements before and after heat treatment. The results were compared with the values given by the supplier. It was apparent that there was virtually no loss of any elements during the austenitizing treatment.

The details of the thermal cycling treatments are given in the following section.

B. Thermal Cycling

1. Conventional and Experimental Heat Treatments

All the samples, initially martensitic as a desirable starting microstructure[7] for grain size refinement, were thermally cycled according to the cycling program shown schematically in Figs. 1 and 2. Figure 1 represents a somewhat idealized experimental cycle in comparison with a reasonably representative conventional austenitizing treatment. In an experimental cycle the samples were heated alternately in the austenite range and two phase ($\alpha + \gamma$) range with intermediate iced brine quenching. When the specimens are put into a tube furnace, kept at a constant temperature, which was controlled within ±5°C, a temperature gradient through the cross section of the specimen sets up until complete transformation occurs. Ideally, as soon as the center of the cross section attains the transformation temperature, the specimens were immediately quenched.

2. Conventional and Experimental Rapid Heat Treatments

Figure 2 shows the experimental rapid thermal cycling method in comparison with a reasonably representative rapid austenitizing treatment for developing ultrafine grain size. Rapidly austenitized specimens were identical in size but were heated rapidly. Rapid heating was accomplished by immersing the specimens in a neutral salt bath kept at a desired temperature. The neutral salt bath was adopted because the desired temperature could be closely controlled and accurately measured automatically. The rapid heat treatment process, originally developed by Grange,[7] consists of repeated cycles of rapid austenitizing

each of very short duration at a temperature barely sufficient to austenitize, and intermediate drop quenching. The thermal cycle profile is identical for the experimental rapid heat treatment, shown in Fig. 2, and the experimental heat treatment shown in Fig. 1 except for the heating rate and duration at peak temperature. Since the solid-state reaction in the alloy system investigated occurs very rapidly, considerable care is required in controlling the interdependent variables, temperature and holding time.

C. Tensile Testing

Tensile properties were determined using the flat tensile specimens shown in Fig. 3. The specimens were originally machined oversize, heat treated and subsequently ground to final dimensions. Approximately 0.012 in. layer for the alloy A was removed from each surface in order to eliminate the possible effects of surface decarburization. Optical microscopic examination revealed that decarburization was not deeper than 0.007 in.

Tensile tests were performed at room temperature in an Instron machine with a cross-head speed of 0.05 cm/min and full scale load of 1000 Kg. Uniform elongation was measured from the stress-strain curve and minor corrections were made with a one-in. extensometer capable of measuring strains up to 60%, the output of the extensometer being fed into the chart drive system of the Instron control console. Values of percent elengation reported are averages of at least three tests. Measurements of each gage section before and after testing were accurately determined using an optical microscope equipped with a vernier translating stage calibrated to 0.001 in.

D. Microscopy

1. Optical Metallography

Sections to be used for optical microscopic observation were cut from the tensile specimens. They were mounted in Koldmount and ground on successively finer papers to 600 grit and then polished on a one micron diamond abrasive wheel lubricated with Kerosene. In these metallographic investigations the standard etchant 2% nital was used; to reveal the prior austenite grain boundaries in quenched samples, an etch solution of 1.4g picric acid, 1g sodium tridecylbenzene sulfonate and 100ml water served satisfactorily.

2. Transmission Electron Microscopy

It was decided to concentrate this investigation mainly on the microstructures and related tensile properties of the alloy "A", since basically there is no significant difference in compositions between them except slight differences in the amount of interstitial solutes (carbon and nitrogen).

The specimens of 0.125 in. thickness for thin foils were heat treated together with the tensile specimens. Each side of the specimens was carefully ground to 30~40 mils thickness. Flood cooling was employed to minimize specimen heating during grinding. The specimens were then chemically thinned to about 5 mils thick in H_2O_2 containing 2% HF at room temperature. Discs of the size of the standard Siemens specimen holder (2.3 mm dia.) were punched and mechanically sanded to 1~2 mils and then electropolished in a twin-jet polishing apparatus

using a chromic-acetic acid solution (75 gms CrO_3 + 400 ml CH_2COOH + 21 ml H_2O). The voltage varied from 25~30 volts. Normal polishing time was about three to five minutes depending on the thickness of the initial disc. Foils were examined in a Siemens Elmiskop IA at an accelerating voltage of 100 kV.

3. Fractography

All fracture surfaces of tensile specimens were examined using a JSM-U3 scanning electron microscope with secondary emission at 25 kV. Fracture surfaces selected for examination were taped to prevent any mechanical damage and contamination by extraneous particles, then stored in dessicators until examined in the scanning electron microscope.

III. RESULTS AND DISCUSSIONS

A. Grain Size Refinement

1. Comparison of Standard and Non-Standard Thermal Cyclings

For many reasons[10-12] the degree of grain refinement becomes more pronounced as the carbon content in a steel alloy increases. Therefore, it is expected that, for alloys A and B, their response to various heat treatments would be rather poor. However, this is desirable for the present purposes, because variables which influence grain size and mechanical properties in steels of such low hardenability are accentuated. The starting microstructure is an important variable in determining the extent of grain refinement by thermal cycling. Speich and Szirmae[12] have shown that the preferred starting structure for carbon steels is a hot rolled structure, whereas Grange[11] reported that martensite or fine ferrite-carbide aggregates qualify as desirable.

In this investigation, martensite was chosen, by quenching from high austenitizing temperature (1100°C) as the initial microstructure. This was partly to minimize possible segregation of embrittling impurity elements into the prior austenite grain boundaries on slow cooling, which as a result might lead to intergranular embrittlement. Therefore, it was necessary to use intermediate quenching rather than slow cooling on subsequent thermal cycling steps (as expected in commercial structural steels, preliminary experiments showed that the tensile properties of the specimens which had undergone the thermal cycling with intermediate air cooling and had finer grains were nevertheless poorer than those of as-received specimens with larger grain size, presumably due to intergranular embrittlement).

The initially martensitic samples, Fig. 4a, were subjected to the thermal cycling treatment shown in Figs. 1 and 2. Extensive isothermal experiments were made, by varying the temperature at fixed holding time and then varying the holding time at constant temperature, to determine the A_3 temperature, the peak temperature and holding time at the peak temperature. Based on optical metallography, the A_3 temperature was found to be 860°C for alloy A and 880°C for alloy B. In order to determine suitable austenitization periods, isothermal experiments were made at 20°C above their respective A_3 temperatures. Insufficient holding time results in undissolved ferrite which can be identified by its "blotchy" appearance in the optical micrograph of an as-quenched specimen; excessive grain growth sets the upper limit. Following these guiding principles of obtaining optimum peak temperature and holding time, the conditions for subsequent steps were also optimized to achieve maximum grain refinement. For specimens A and B subjected to conventional heat treatment, a suitable austenitizing time was found to be six minutes for the first cycle (C1) and five minutes for the second cycle (C2), producing (after C2) microduplex structures consisting of mainly martensite and proeutectoid ferrite (Fig. 4b). The lower half of the Fig. 4b shows the prior austenite grain boundaries revealed by an etch solution mentioned previously and the upper half of it was obtained using standard 2% nital. Both of them were taken from the same heat treated specimen (C2). For the experimental heat treatment, the annealing temperature in the two phase ($\alpha + \gamma$) range was chosen at 20°C below the A_3 temperature for alloy A, and at 30°C below A_3 for alloy B. The optimum annealing time in the ($\alpha + \gamma$) range

was found to be 7 minutes and 5 minutes for the cycles T2 and T4 respectively. The grain size achieved after heat treatment T2 is shown in Fig. 4c, illustrating that carbon enriched austenite, produced by partitioning in the two phase field, transformed to martensite as evidenced by dark etching. The proeutectoid ferrite appeared as the light etching constituent and remained untransformed during quenching. Similarly, for rapid heat treatment, the austenitizing time at the peak temperature was determined to be 40 seconds in the first cycle (RC1) and successively shorter times 38, 33 and 30 seconds for RC2, RC3 and RC4 heat treatments respectively to bring about the structures shown in Fig. 5a (RC2) and Fig. 6a (RC4). For experimental rapid heat treatment, optimized annealing times in the two phase field were found to be 39 and 32 seconds for RT2 and RT4 respectively. As a result, the microduplex structures are illustrated in the composite picture given in Fig. 5b (RT2) and Fig. 6b (RT4).

The samples subjected to single-cycle austenitization were found to have a severely duplexed grain structure. Thus, in order to make meaningful comparisons of grain sizes and mechanical properties in each thermal cycling technique, only the specimens which had undergone second and fourth cycles were investigated. Grain sizes were measured by linear intercept method from optical micrographs and the results are given in the Figure captions. As may be seen in Figs. 4 through 6, most of the microduplex structures showed fairly uneven grain size distribution throughout the samples. Presumably this is due to the existence of proeutectoid ferrite inevitably present because of low hardenability, and due to the presence of nonuniform carbide morphology

(see Fig. 15). This would lead to more grain refinement in some areas than others, since the nucleation of the $\alpha \rightarrow \gamma$ transformation on heating is usually believed to be precipitate-correlated.[12] It is also noted that the shapes and features of the grains are quite distinctive. For example, some blocky ferrite mixed with austenite grains are shown in Fig. 4c, and carbon enriched γ islands in the matrix of α are seen in Fig. 6b and so on. In these respects, the average grain size measurement for the specimens is probably a poor approximation of the effective grain diameter.

Above two cycles, further reduction in grain size by slow heating methods (in comparison with rapid heat treatment) did not occur, demonstrating the limitations of developing substantially finer grain size by the above heat treatments. The grain size (~18μ , ASTM #9) obtained by heat treatment RC2 suggests that rapid heat treatment does not provide significant improvement in grain size refinement over conventional methods (24μ, ASTM #8) in the alloy investigated. Presumably this is due to the uneven carbide distribution and the presence of proeutectoid ferrite as described before. Furthermore, no appreciable change in grain size was observed with two more cycles (heat treatment RC4, Fig. 6a) after the second cycle in this investigation. Figures 4 to 6 and the grain size data in the figure caption illustrate that the experimental heat treatments, T and RT provide finer grain sizes (though not pronounced) than those obtained by conventional (C) and rapid heat treatments (RC), respectively. It appears that the second phase (proeutectoid ferrite) may effectively inhibit grain growth of austenite in the two phase field.

B. Microstructural Changes on Thermal Cycling

The various ferrite, martensite and carbide morphologies encountered with each of the thermal cycling treatments were examined using transmission electron microscopy techniques. The most significant feature in all the as-quenched specimens, except the starting microstructure, was the microduplex structure consisting mainly of proeutectoid ferrite and martensite, each amount depending on the specific heat treatment and the number of cycles. After careful visual examination of many electronmicrographs and optical micrographs the approximate fraction of martensite was determined. These relative values of some selective heat treatments are given in Table 2.

1. Morphology of Martensite

The typical features of martensite in the low carbon steel are shown in Figs. 7 through 9. The microstructure consisted almost entirely of dislocated laths of the order of 0.1μ~0.5μ wide; however, much thicker laths, a few microns wide exist in some areas, as shown in Fig. 10. There were also present a small number of martensite plates within the structure. In these areas there was sometimes evidence of internal twinning free of carbide (Fig. 9a). The martensite plate, such as the one shown in Fig. 8b was often seen to be composed of several subunits. Adjacent laths are sometimes twin related (Fig. 9b) or separated by small angle boundaries. Another prominent feature of the martensite was the occurrence of autotempering. The density of the autotempered carbides was highest in the starting

microstructure and decreased remarkably in the specimens after two cycles. Negligible amounts of autotempered carbides were present after 4 cycles. The reason for this may be that the specimens subjected to thermal cycling always contained some undissolved carbides with the % undissolved carbide increasing with additional cycles. Any additional carbon in solution was probably segregated to lattice defects during quenching[13,14] since most of these sites have a lower energy than those available at the precipitate,[15] so there is little driving force for precipitation in the martensite.

The characteristics of the martensite morphology in the low carbon steels described above are quite common and are similar to those first reported by Kelly and Nutting.[16,17] Examples of the autotempered carbide morphology are shown in Figs. 10 and 11. Since the carbide diffraction spots were very weak, the carbides were tentatively identified by trace analysis. Most of the carbides were cementite, in typical {110} Widmanstatten orientation. Figure 10a shows precipitation of autotempered cementite and Fig. 10b is a {110} dark field of the same area as Fig. 10a in the initial specimen. The Widmanstatten cementite precipitates in the specimen A4 (heat treatment C2+IBQ) are shown in Fig. 11. No observable difference in the morphologies of carbides in each thermal cycling treatment was found. However, precipitation of cementite in the specimens subjected to the repeated austenitization (conventional or rapid heat treatment) was more dense than that in the specimens subjected to two phase decomposition. Presumably this is because the former methods provide more opportunity for carbon to dissolve by annealing at a higher temperature and more

effectively annihilating the defect structures, especially dislocations, which allow favorable sites for carbon segregation.

An important observation was the existence of extremely narrow films of retained austenite around the martensite laths (see Figs. 16, 17 and 18), the amount depending upon heat treatment. This will be discussed further in a later section. There were also indications of lath-boundary carbide precipitation as shown in Figure 12. However, this auto-tempering was neither widespread throughout the structure nor in great amounts. Figure 12b shows a dark field micrograph showing reversal of contrast of lath-boundary carbides which cannot be easily recognized in the bright field image (Fig. 12a). The carbides were identified as cementite from selected area diffraction patterns (Figs. 12c and d). The crystallographic relationship between the cementite and ferrite matrix corresponded to the Bagaryatskii orientation relationship which has already been pointed out,[18] and is as follows:

$$[100]Fe_3C \parallel [0\bar{1}1]\alpha$$

$$[010]Fe_3C \parallel [1\bar{1}\bar{1}]\alpha$$

$$[001]Fe_3C \parallel [211]\alpha$$

2. Morphology of Ferrite and Carbide Distribution

The 0.5% Mn, 0.12% C steel is hypo-eutectoid in composition, and has very low hardenability; thus, pro-eutectoid ferrite followed by precipitation of (α + carbide) according to the $\gamma \rightarrow \alpha$ + carbide reaction should be expected at high transformation temperature upon quenching. The ferrite regions in all the specimens subjected to the various heat

treatments were locally heavily dislocated. However, the significant differences in proeutectoid ferrite morphologies between specimen A4 (heat treatment C2 + IBQ) and specimen A5 (T2 + IBQ) were subgrain size and dislocation density. In specimen A4, the high density of dislocations, introduced to accommodate the $\gamma \rightarrow$martensite transformation strain in the ferrite regions upon quenching, would appear to have been reduced by self annihilation and subsequently annealed out on heating, since the structures change as the $\alpha \rightarrow \gamma$ transformation proceeds. Thus, in this structure the dislocations were mostly fresh dislocations produced in the last step of quenching in the heat treatment sequence. Moreover, the dislocations were frequently concentrated in the vicinity of the α/martensite boundaries. This is illustrated in Fig. 13a.

On the other hand, the proeutectoid ferrite in the specimens A5, subjected to two phase decomposition, forms without undergoing any phase transformation when α is annealed in the two phase region. As a result, the dislocations generated by partial martensitic transformation on quenching would rearrange themselves into dislocation walls, thus forming sub-boundaries during annealing in the two phase field. This is shown in Figs. 14 and 15. This, in turn, may influence the tensile properties and will be discussed in a later section. The electron microscopy examination revealed that the specimens subjected to heat treatment T2 contained sub-boundaries spaced on average 1 to 2μ apart (Fig. 14c) in some areas, and much larger size than this in other areas (Fig. 14a and b), whereas specimens A4 (repeated austenitization) exhibited much less subgrain structure.

Another significant feature of the ferrite regions was the high degree of inhomogeneity of two types of precipitation as shown in Figs. 14 and 15. The ferrite areas associated with very fine distribution of precipitates, possibly carbides and/or nitrides, were frequently observed in the specimens A5 but not so often in specimens A4. It is speculated that the origin of the fine precipitates (Fig. 14b) arises from a supersaturation of carbon and nitrogen, and that in the specimens A4 the outward diffusion of the interstitial solutes might cause depletion of carbon in the proeutectoid region (see Fig. 15a, upper left) as a proeutectoid ferrite grain nucleates and grows into austenite grains. The ferrite in the immediate vicinity of the martensite/α boundaries showed a high density of carbide particles resulting from the $\gamma \rightarrow \alpha$ + carbide reaction after the completion of the nucleation and growth of proeutectoid ferrite upon quenching. This is illustrated in Fig. 15. This type of structure was frequently observed in all the specimens observed, and is similar[19] to that observed in the isothermal decomposition of austenite in Cr steels. The diffraction patterns obtained from the structure were so complex that the carbides could not be identified unambiguously. However, Campbell and Honeycombe[19] suggested that the carbides are of M_7C_6 type (or more strictly $(Mn,Fe)_7C_6$ in this case). It was difficult to see where and when the individual carbides had nucleated. It appears that the carbide adopted both a fibrous morphology (Fig. 15d) in which the prior γ/α interfaces are heavily faceted, and an interface precipitation morphology (Figs. 15a and c) where the interfaces are largely smooth. The prior γ/α interfaces seem devoid of carbide precipitates. This can be shown by dark field

microscopy e.g., Fig. 15(b).

The zone of the localized carbides was 1 to 3μ wide. It is speculated that this heavy precipitation of carbides would result in detrimental effects on tensile properties, and provide preferential nucleation sites[12] for γ, thus producing inhomogeneous grain size and irregular distribution of fine precipitates (Fig. 14). As the number of heat cycles increases, the zone was reduced remarkably presumably due to the increased retention of carbon in carbides and lattice defects with each successive cycle and, therefore, less available carbon to form carbides.

C. Formation of Retained Austenite

It was interesting to observe retained austenite in an alloy with such low carbon, since to our knowledge no reports on this are in the literature. All the specimens observed revealed retained austenite that was trapped between two growing martensite laths in the form of narrow thin films. The extent depended on the heat treatment and number of cycles. This is illustrated in Figs. 16 through 18.

The stabilization of austenite has been the subject of a number of investigations. Austenite retention at room temperature can be explained partly by the lowering of M_f temperature below room temperature due to carbon enrichment. Its retention can also be understood in terms of thermal and mechanical stabilization.[17,22] Thermal stabilization is attributed to modifications of the untransformed austenite where the dislocations in the austenite lattice are locked by solute atmospheres. As a result, the structure is hardened, and the cooperative movement of atoms necessary for further martensitic

transformation may be inhibited. Mechanical stabilization is caused by the strengthening of austenite due to external plastic deformation or to accommodation deformation resulting from transformation stresses.

In applying these concepts, it seems plausible that retained austenite should form in a low carbon steel. Figure 16 shows an example of retained austenite trapped between martensite laths in the starting microstructure and Fig. 16b is the dark field micrograph where the retained austenite reverses contrast. Selected area diffraction patterns such as the one given in Fig. 16c were used to identify the presence of retained austenite. Figure 16d shows the crystallographic relation between austenite and martensite, which exhibits the Kurdjumov-Sachs orientation relationship, $\langle 111 \rangle_\alpha \parallel \langle 110 \rangle_\gamma$. Another interesting observation was that the specimens given alternate thermal cycling (T2 and RT2) revealed more retained austenite than those given repeated austenitization (C2 and RC2). It seems that the increase in retained austenite may result from an increased lattice distortion due to higher transformation strains in the carbon enriched austenite produced by two phase decomposition. The retained austenite in the specimen A5 is shown in Fig. 17, where some carbides also reversed contrast in the dark field image. This occurs since the carbide spots are sometimes very close to fcc austenite spots, particularly when a $(111)_\gamma$ spot is used to take dark field micrographs.

In order to see whether or not retained austenite was stabilized thermally or mechanically, specimens A5 were refrigerated in liquid nitrogen (-196°C) for 1 hr immediately after the iced brine quench.

Examination of many thin foils showed that approximately half of the retained γ present in the specimens A5 was reduced in the specimens transferred to liquid nitrogen (Figs. 18a and b). This shows that the retained austenite was subject to both thermal and mechanical stabilization. However, it was impossible to obtain quantitative data on the exact amount of retained γ by X-ray analysis.

It seems likely that the amount of retained γ should decrease as the number of thermal cycle increases since carbon retention by the carbides and at defects should increase. However, considerable amounts of retained γ were observed (Figs. 18c and d) in the specimens after four cycles (heat treatments RC4 and RT4), and there was no observable difference in the amount of retained γ between the specimens A11 and A12. This can be understood if the residual strain from the cyclic shear transformation is allowed to accumulate since both the direct and the reverse transformations during thermal cycling treatment result in deformation of the surrounding material. Thus the effect of the residual strain on the formation of retained austenite may be a more dominating factor than the difference in the carbon concentration of the austenite, resulting in no observable difference in the amount of retained austenite between specimens A11 and A12 as mentioned above.

D. Relation between Microstructures and Tensile Properties

The room temperature tensile tests data are summarized in Table 2 and Fig. 21. From these, it is noted that 1% increase in the uniform elongation is accompanied by about 7~10 ksi drop in yield strength.

Figure 21 shows the plot of yield strength vs. uniform elongation for the specimens A1, A2 and A4, and A1, A3 and A5. The values of uniform elongation resulting from the heat treatment (T) are shown to be better at similar strength level than those from the conventional heat treatment (C). Comparing the values of yield strength and uniform elongation of the specimens A4 and A5, for example, one observes that there is 2% increase in the uniform elongation in specimen A5 over A4, while the drop in yield strength is small, and specimens B2 and B3 show a 3% difference in uniform elongation at the same strength level. It can be noted that yield strength is more sensitive than ultimate tensile strength to the different heat treatments. Table II shows that in general the heat treatment investigated in this research provided better combinations of yield strength and uniform elongation than repeated austenitization. In addition, there is no significant advantage resulting from rapid heating techniques (e.g., heat treatments RC2 and RT2) than slow heating methods (e.g., C2 and T2).

The superior combinations of yield strength and uniform elongation resulting from the heat treatment T2 should be understood in terms of the substructural and morphological differences between specimens A5 (heat treatment T2+IBQ) and A4 (C2+IBQ). The following parameters appear to be important: (a) fraction of martensite, (b) the prior austenite grain size, (c) dislocation substructure, (d) distribution of fine precipitates, and (e) retained austenite.

Of these, fraction of martensite seems to be most influential on yield strength and uniform elongation as shown in Table 2. Tensile test data obtained from specimens A1, A2 and A4 show an almost linear increase in yield strength and a roughly linear decrease in uniform elongation with increasing amount of martensite. Similar trends are observed from specimens A1, A3 and A5. Comparing specimens A2 and A3, and also A4 and A5 one can see that A3 and A5 exhibit 15~20% less fraction of martensite and a 2% increase in uniform elongation with respect to specimens A2 and A5 respectively. Nevertheless, the values of yield strength are similar. This can be observed in almost all the tensile test data of the specimens given non-standard thermal cycling treatments in comparison with those of the specimens subjected to corresponding conventional thermal cycling treatments including rapid heat treatments as shown in Table 2. Thus it appears that a 2~3% increase in uniform elongation in the specimens given non-standard heat treatments arises mainly from a smaller fraction of martensite, viz, higher amount of soft phase ferrite than that in the specimens given standard heat treatments. In other words, this means that the former specimens have to be strengthened additionally from the other sources in order to achieve similar strength level with that of the latter specimens which have higher amounts of martensite as mentioned before.

The parameters described previously seem to be responsible for the strengthening sources. Firstly, grain size effect; for a number of metallic polycrystalline aggregates, it has been shown experimentally that σ_f, the flow stress at constant strain, is related to the grain diameter D by the Hall-Petch equation

$$\sigma_f = \sigma_0 + kD^{-1/2} \qquad (1)$$

where σ_0 is the shear stress required to cause slip to occur in the absence of grain boundary resistance and k is a measure of the stress concentration which is generated at the tip of a slip band.

It is customary to measure and express the grain diameter of steels as the grain size of the austenite[4,7] developed prior to cooling to room temperature in the final heat treatment, since ferrite grain size tends to become experimentally indeterminate.[7] As mentioned before, the experimental heat treatments provided finer prior γ grain size than can be attained by other heat treatments, hence this may contribute to the improved tensile properties. However, since the decrease in the grain size was not great the contribution, if any, would be small.

Warrington[23] and Baird[24] reported that the equation (1) can be applied to the effect of subgrain size on the flow stress of iron. As described previously, since the ferrite region in the specimen A5 involved ultrafine subgrains (though not distributed evenly), the ferrite would be effectively strengthened according to equation (1).

Variation in carbide morphology with different heat treatments may also have an effect on the properties. However, positive proof was not available since the distribution of the precipitates was very irregular.

Retained γ is known to influence a variety of properties, but the way in which the presence of retained γ aids in improving these properties is not completely clear at this time. However, the beneficial effects of small amounts of retained austenite on the mechanical properties have been

reported by many investigators.[1,25] All the specimens A6 (A5 + refrigeration at LN) exhibited smaller values of uniform elongation (though not pronounced) than specimens A7, possibly due to the reduced retained γ as described before. However, the differences were very small, therefore, the effect of retained γ on the improved properties is expected to be very small.

All the variables mentioned above acting in concert could have accounted for the observed tensile properties and in this investigation it was not possible to isolate their individual effects. More work needs to be done to establish uniquely the role of each on the properties.

The tensile properties of the specimen given 4 cycles (C4, T4, RC4 and RT4) revealed some deviations from what is expected, possibly because of the heat treating conditions (the rapid heat treatment technique is very sensitive to the holding time and peak temperature) and the interaction of many variables such as carbide distribution, grain size, percent martensite etc. However, the only qualitative conclusion that could be arrived at from the results is that multicycling more than 2 cycles did not provide additional improvement in tensile properties.

All the observed fracture surfaces showed no apparent change in fracture mode with different heat treatments except the specimens A1 which exhibited small dimples mixed with quasi-cleavage-like areas (Fig. 19). Figures 20a and b illustrate the typical fracture morphologies of specimens A4 and A5 respectively, where no significant differences in fracture mode could be observed. An additional feature of the fractographs was that the fracture surfaces were associated with inclusions which might act as nucleation sites for void nucleation, and hence provide easy crack propagation.

IV. CONCLUSIONS

Based on various heat treatments which were investigated, the following conclusions are drawn:

1. The heat treatments investigated provided a better refinement in grain size compared to that from conventional heat treatments. It appears that proeutectoid ferrite may effectively inhibit grain growth of austenite.

2. Multicycling more than two cycles did not provide additional grain refinement, nor did it provide additional improvements in tensile properties.

3. The ferrite region of the specimens subjected to the experimental heat treatment seemed to be effectively strengthened mainly by the formation of ultrafine subgrains.

4. Better combination of yield strength and elongation ductility could be achieved.

5. There was no apparent advantage accrued through rapid heat treatment in the alloy system investigated.

6. It is suggested that the beneficial heat treatments arrived at in this research ideally combine the beneficial effects of finer grain size, dislocation substructure, distribution of fine precipitates in ferrite regions, and retained asutenite.

7. As described before, a high density of carbide particles in the immediate vicinity of the martensite/α boundaries appears to be detrimental to tensile properties. Therefore, it is suggested that the addition of alloying elements such as silicon and aluminum which are known to inhibit the growth of carbides,[20,21] might improve the mechanical properties.

ACKNOWLEDGEMENTS

The author is deeply grateful to Professor Gareth Thomas for his continued guidance and encouragement throughout the course of this work. Dr. G. W. Bailey and General Motors Research Laboratories graciously supplied the alloys used in this research. Appreciation is also extended to Dr. Sungho Jin for many helpful discussions.

This work was done under the auspices of the U. S. Energy Research and Development Administration through the Inorganic Materials Research Division of the Lawrence Berkeley Laboratory.

REFERENCES

1. G. Thomas, Iron and Steel International, 46, 451 (1973).
2. G. Y. Lai, W. E. Wood, R. A. Clark, V. F. Zackay and E. R. Parker, Met. Trans., 5, 1663 (1974).
3. S. K. Das and G. Thomas, Trans. ASM, 62, 659 (1969).
4. W. C. Leslie, "Strengthening Mechanisms", 12th Sagamore Army Materials Research Conference, p. 43 (1965).
5. K. J. Irvine, JISI, 820 (1962).
6. R. L. Smith, et al., Trans ASM, 46, 973 (1954)
7. R. A. Grange, Trans. ASM, 59, 26 (1966).
8. S. Jin, Ph.D. Thesis, University of California, 1974.
9. E. Snape and N. L. Church, Journal of Metals, p. 23 Jan.(1972)
10. B. Karlsson, Mat. Sci. and Eng., 11, 185 (1973).
11. R. A. Grange, Met. Trans., 2, 65 (1971).
12. G. R. Speich and A. Szirmae, Met. Soc. AIME, Trans., 245, 1063 (1969).
13. G. S. Ansell, et al., Met. Trans., 2, 2443 (1971).
14. G. R. Speich and W. C. Leslie, Met. Trans., 3, 1043 (1972).
15. D. Kalish and M. Cohen, Mat. Sci. Eng., 6, 156 (1970).
16. P. M. Kelly and J. Nutting, Proc. Roy. Soc. London, A259, 45 (1960).
17. P. M. Kelly and J. Nutting, JISI, 197, 199 (1961).
18. D. N. Shackleton and P. M. Kelly, The Iron and Steel Inst. (London), Report 93, 126 (1965).
19. K. Campbell and R. W. K. Honeycombe, Metal Sci., 8, 197 (1974).
20. J. M. Oblak and R. F. Hehemann, Transformation and Hardenability in Steel, p. 15, Climax Molybdenum Co., Ann Arbor, 1967.

21. W. S. Owen, Trans. ASM, 46, 812 (1954).

22. J. W. Christian, The Theory of Transformations in Metals and Alloys, Pergamon, New York, 1965.

23. D. H. Warrington, JISI, p. 160 July (1963).

24. J. D. Baird, JISI, p. 44 Jan. (1966).

25. S. D. Antolovich, et al., Met. Trans., 5, 623 (1974).

26. M. Hansen, Constitution of Binary Alloys, 2nd ed., McGraw-Hill New York, p. 357 (1958).

Table 1. Chemical Compositions of Alloys

Alloy	Thickness	composition, wt. % C	Mn	S	N	P
INNA	0.125 in.	0.12	0.49	0.012	0.011	0.004
1010	0.115 in.	0.08	0.46	0.024	0.006	

Table 2. Tensile Test Summary

Heat Treatment	Final Quench	Specimen Number*	Yield Strength** (KSI)	Tensile Strength (KSI)	Uniform Elongation (%)	Estimated Fraction of Martensite (%)
CO†	IBQ	A1	148	174	2	100
		B1	104	118	4	
C2	IWQ	A2	76	112	7	55
T2	IWQ	A3	78	111	9	45
C2	IBQ	A4	101	130	4	75
		B2	71	100	7	
T2	IBQ	A5	97	130	6	60
		B3	71	100	10	
	IBQ+LN	A6	95	130	5	
RC2	IBQ	A7	103	139	5	
		B4	76	106	6	
RT2		A8	95	137	7	
		B5	71	105	9	
C4	IBQ	A9	88	130	6	
		B6	71	102	9	
T4		A10	97	135	5	
		B7	70	100	8	
RC4	IBQ	A11	103	137	4	
		B8	72	103	7	
RT4		A12	95	134	7	
		B9	70	103	9	

*A refers to alloy A, and B to alloy B.

**0.2% upset.

†Starting microstructure.

FIGURE CAPTIONS

Fig. 1. Schematic representation of experimental thermal cycles in comparison with conventional heat treating cycles, referred to part of the Fe-C equilibrium phase diagram.

Fig. 2. Schematic representation of conventional and experimental rapid heat treating cycles.

Fig. 3. Dimensions of a tensile specimen

Fig. 4. Opitcal microstructures. 2% nital etch.

(a) Initial microstructure (martensite), grain size 80μ (ASTM # 3 1/2). Black dots are etch pits.

(b) Specimen A4 (heat treatment C2), 25μ (ASTM #8), lower half: same specimen, but with different etching solution,

(c) specimen A5 (T2), 18μ (ASTM #9).

Fig. 5,6. Optical microstructures consisting of martensite and pro-eutectoid ferrite. 2% nital etch.

(5a) specimen A7 (heat treatment RC2), 18μ (ASTM #9). Right half: with different etching solution to reveal the prior γ grain boundaries.

(5b) specimen A8 (RT2), 10μ (ASTM # 10 1/2),

(6a) specimen A11 (RC4), 16μ (ASTM #9),

(6b) specimen A12 (RT4), 10μ (ASTM # 10 1/2).

Fig. 7. Transmission electron micrograph of specimen A1, showing typical dislocated martensite of low carbon steels.

Fig. 8. Martensite of specimen A5 (a) and A1 (b and c). Auto-tempered carbides are seen.

Fig. 9. Martensite showing a region of fine twins in specimen A5 (a). Twins were observed in most of the specimens subjected up to 2 cycles, but in extremely small amount. (b) Neighboring laths were sometimes twin related.

Fig. 10. Bright field (a) and dark field (b) of auto-tempered carbides in specimen A1, showing the carbides in a Widmanstatten pattern on $\{110\}\alpha$ planes.

Fig. 11. Another region showing auto-tempered carbides in specimen A4.

Fig. 12. Bright field (a) and dark field (b) of lath boundary carbides in the region of as-quenched martensite in specimen A5. Dark field (b) reverses contrast of carbides. (c) Selected area diffraction pattern of the carbides in (a). (d) The carbides were identified as Fe_3C by the indexing of diffraction pattern (c).

Fig. 13. Dislocations introduced in proeutectoid ferrite probably due to the $\gamma \rightarrow$martensite transformation strain.

(a) specimen A4 (heat treatment C2).

(b) specimen A5 (T2).

Fig. 14. Dislocation substructures in ferrite regions of specimen A5.

(a) dislocations rearranged to form a sub-boundary.

(b) sub-grains with very fine precipitates.

(c) sub-grains spaced on an average 0.5μ to 1μ wide. Areas of same contrast have the same orientation.

Fig. 15. Morphology of heavy precipitation of carbides in the immediate vicinity of α/ prior γ boundaries. Carbides of M_7C_3 type in specimen A4 are shown in bright field (a). Dark field (b) shows reversal of carbide contrast.
(c) another region of heavy precipitation of carbides in specimen A4. α/γ interfaces are mostly smooth.
(d) pearlitic type carbides in specimen A5. α/γ interfaces are faceted.

Fig. 16. (a) Bright field image of retained γ trapped between two martensite laths. A FCC austenite spot reversed contrast in dark field (b).
(c) SAD of (a). A FCC spot is marked by image of objective aperture.
(d) Indexing of the diffraction pattern in (c). The crystallographic relation between martensite and austenite correspond to the Kurdjumov-Sachs orientation relationship, $\langle 111 \rangle_\alpha$ // $\langle 110 \rangle_\gamma$.

Fig. 17. Retained austenite in specimen A5. Some carbides also reversed contrast in dark field (b) due to superposition of a carbide spot with a FCC γ spot. The retained γ was present more in specimen A5 than A4.

Fig. 18. Bright field (a) and d.f. (b) of retained austenite in specimen A6. (c) and (d) show b.f. and d.f. images of retained γ in specimen A11 respectively.

Fig. 19. Fractograph of specimen A1 (starting microstructure), showing mixture of small dimpled rupture and quasi-cleavage like areas. Inclusions were located at the bottom of the dimples.

Fig. 20. Fractographs of specimen A4 (a) and specimen A5 (b).

Fig. 21. The values of uniform elongation are plotted against yield strength for the specimens subjected to conventional and experimental heat treatments.

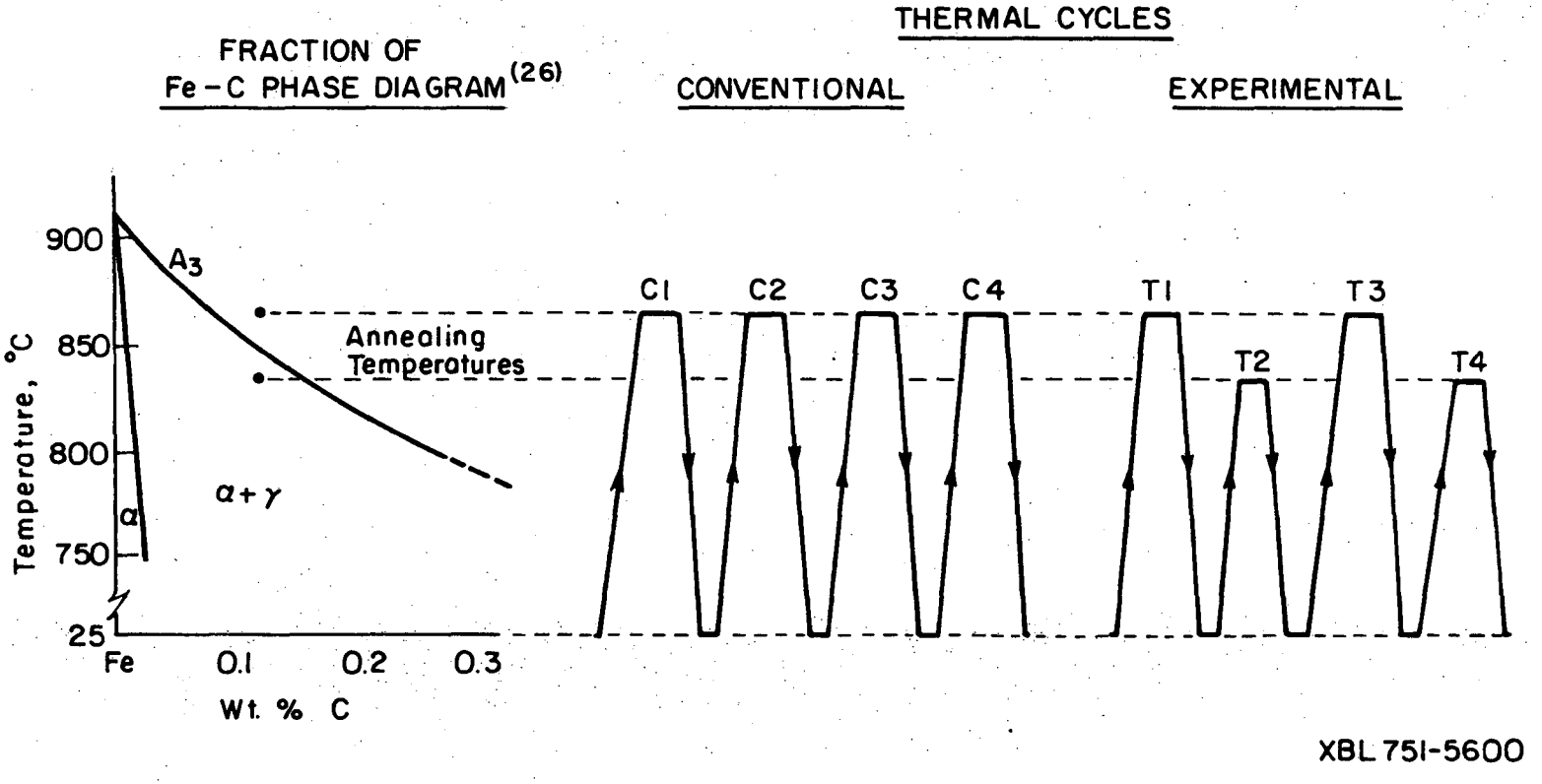
THERMAL CYCLES
FRACTION OF
Fe-C PHASE DIAGRAM(26)
CONVENTIONAL
EXPERIMENTAL
900
850
800
750
25
Temperature, °C
A3
Annealing
Temperatures
α+γ
α
Fe
0.1
0.2
0.3
Wt. % C
C1
C2
C3
C4
T1
T2
T3
T4
XBL 751-5600

Fig. 1

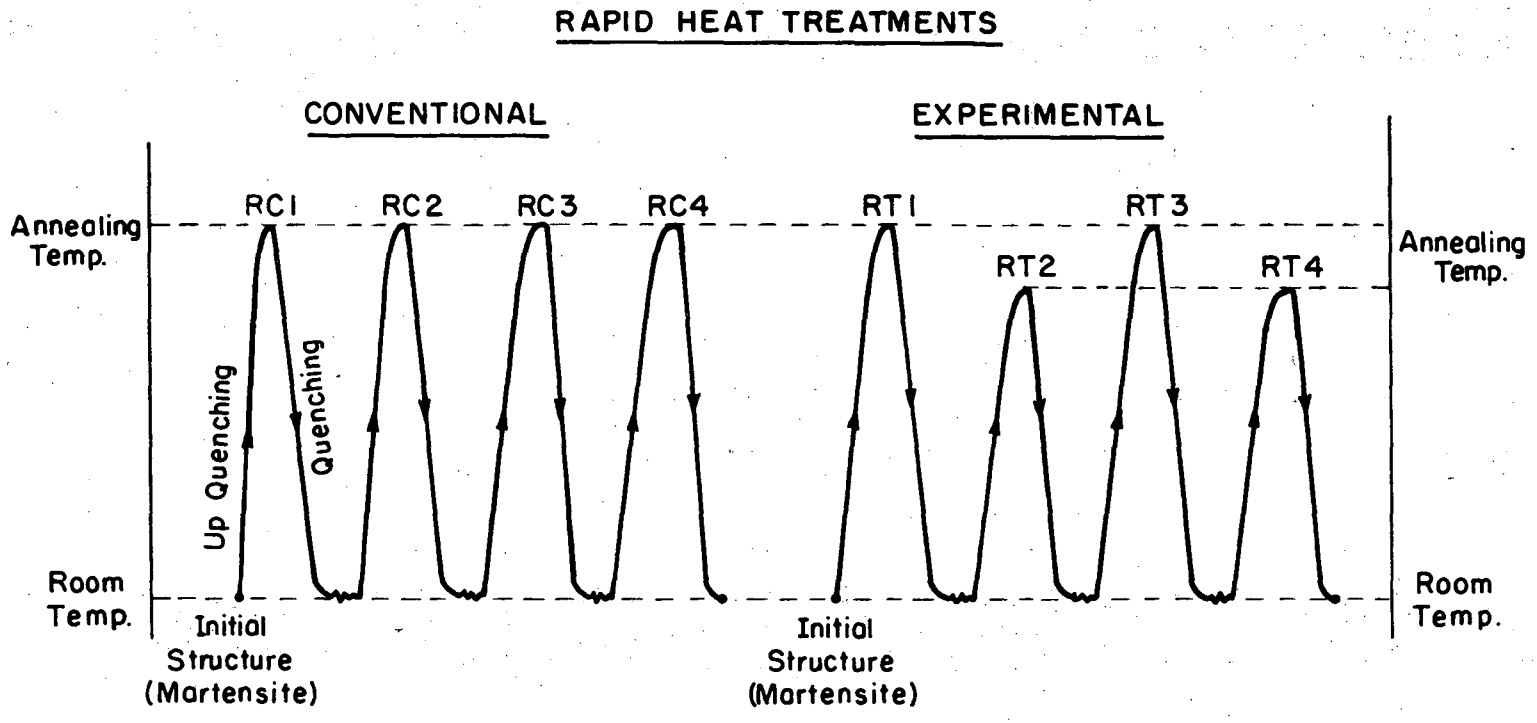

Fig. 2

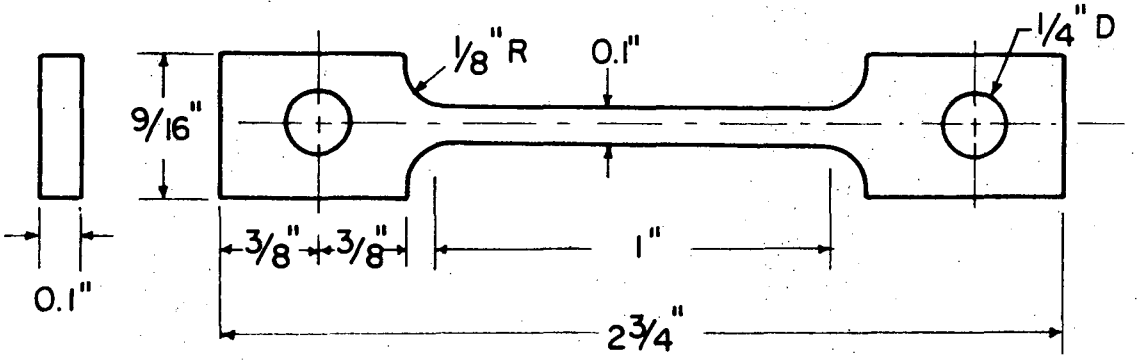

Fig. 3

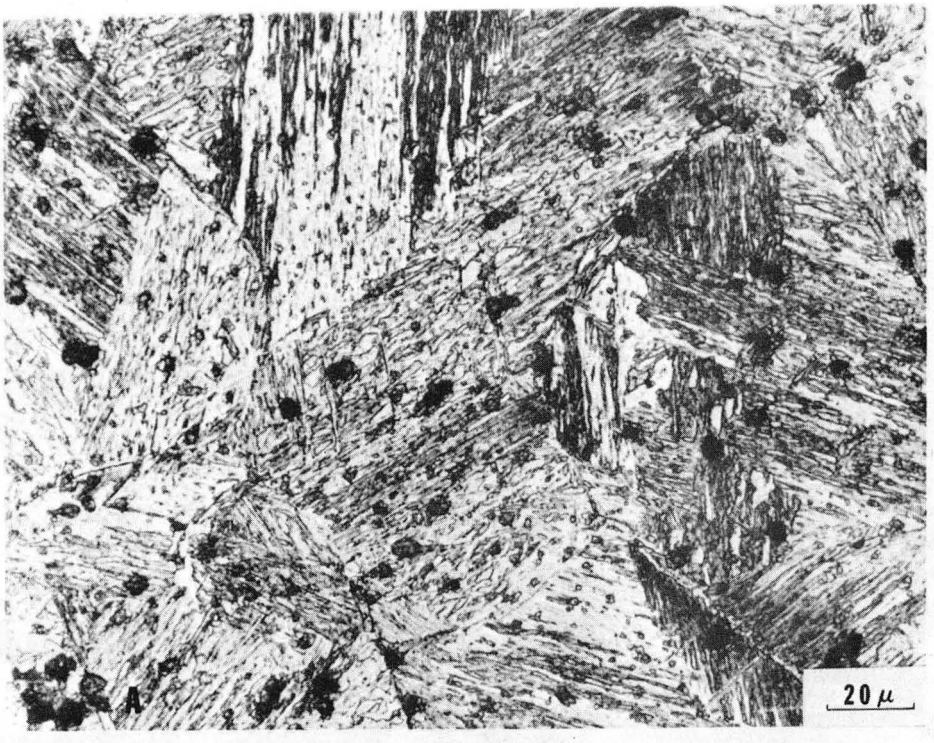

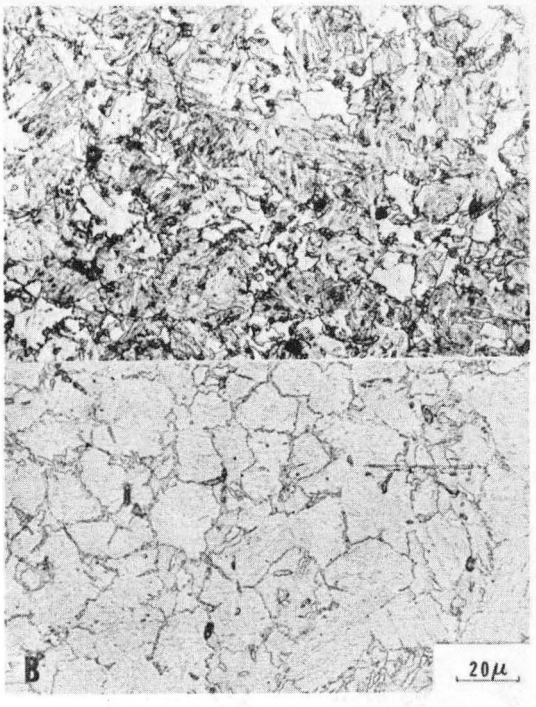

XBB 751-759

Fig. 4

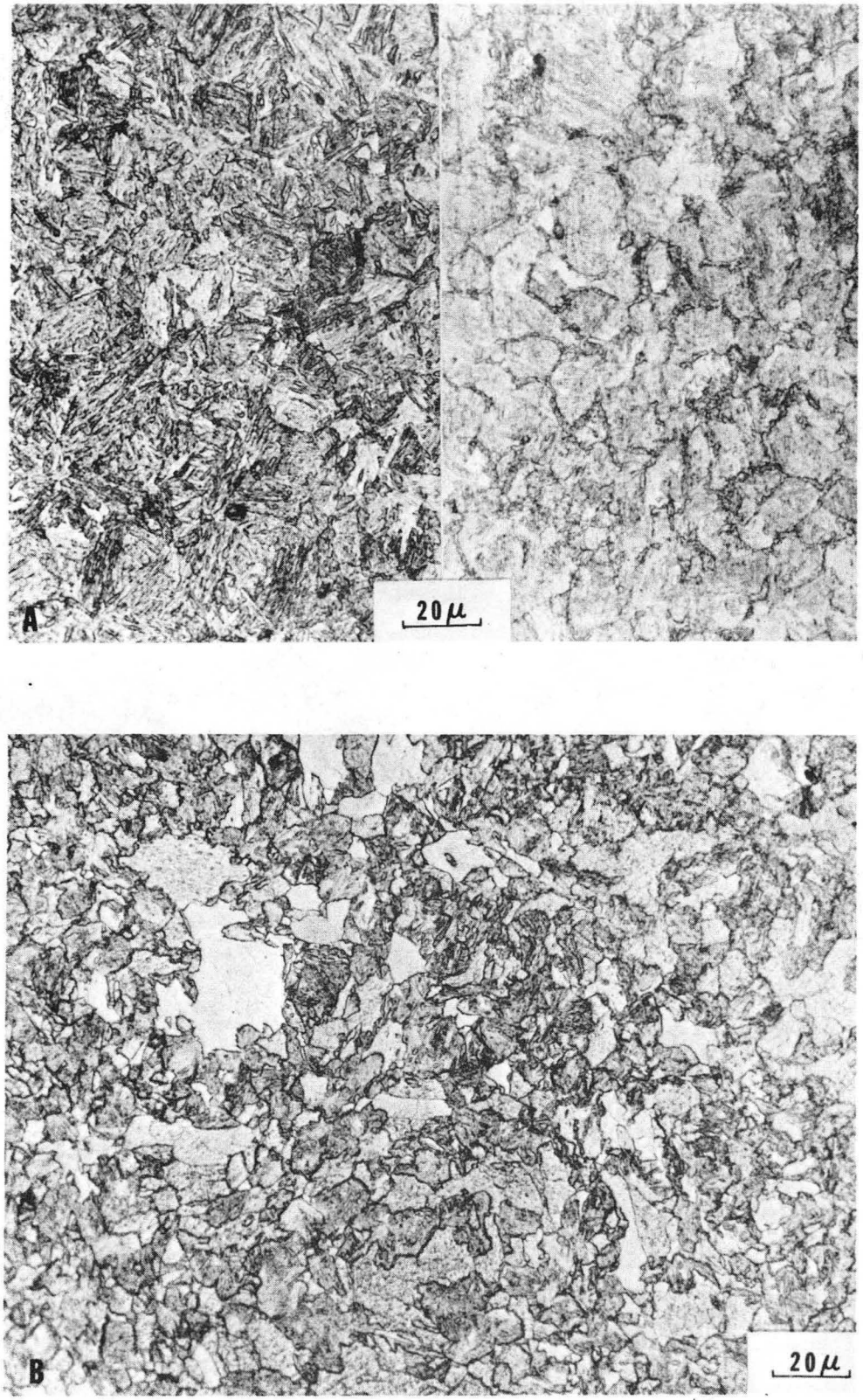

XBB 751-756

Fig. 5

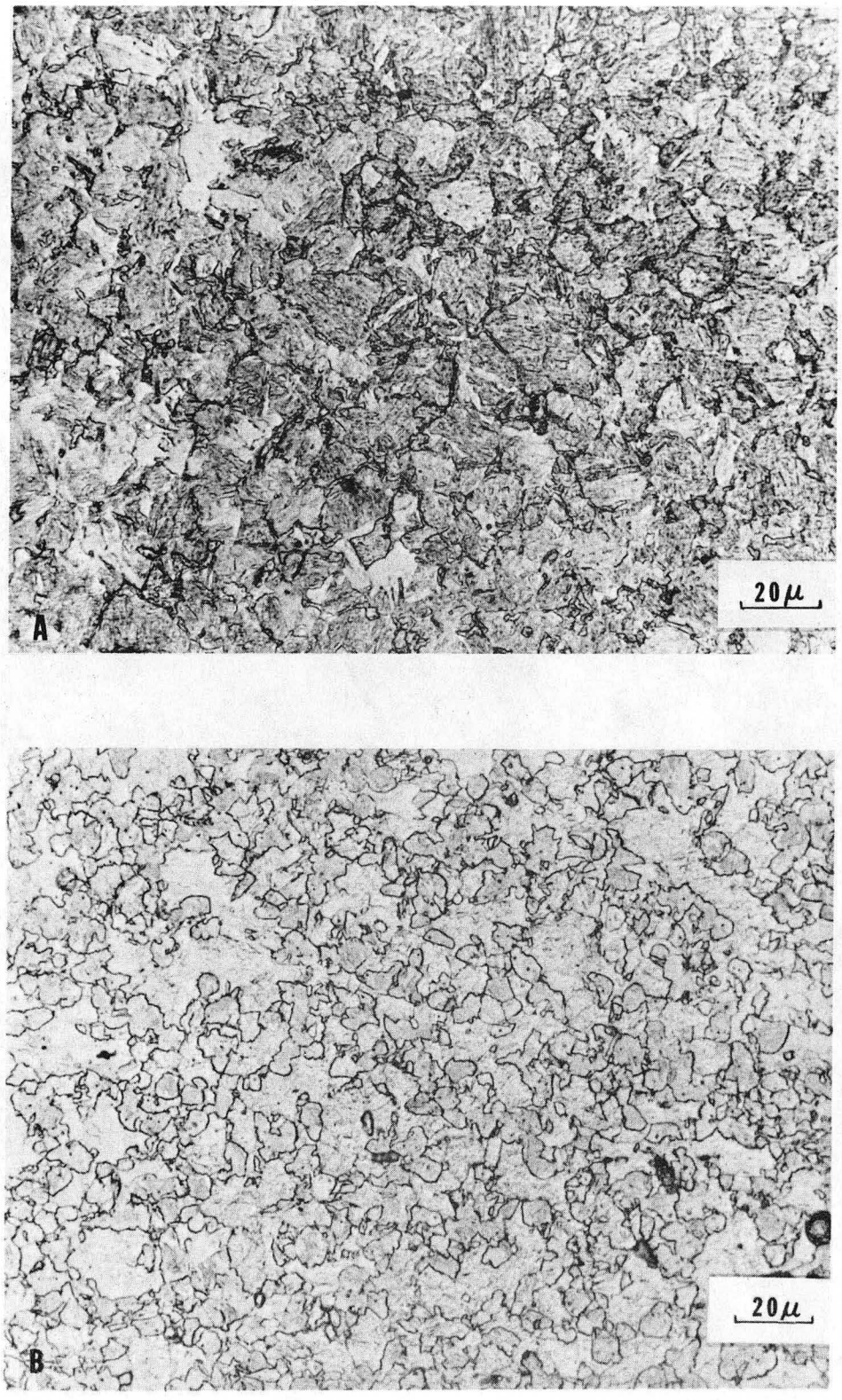

XBB 751-757

Fig. 6

XBB 751-763

Fig. 7

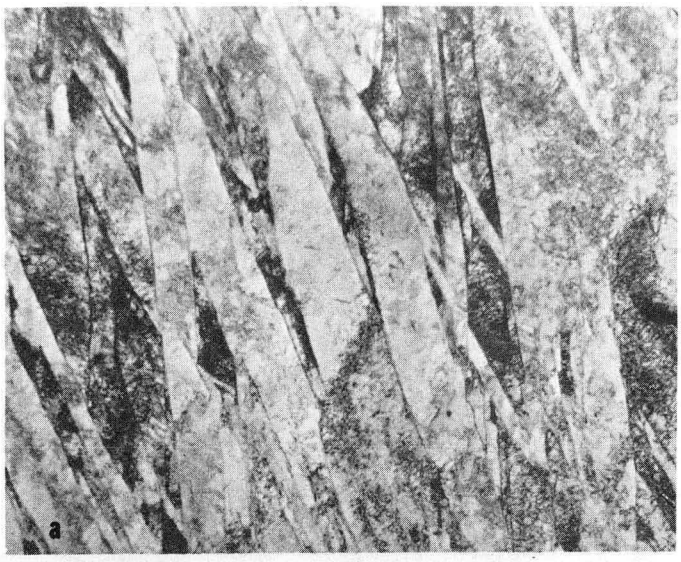

XBB 751-760

Fig. 8

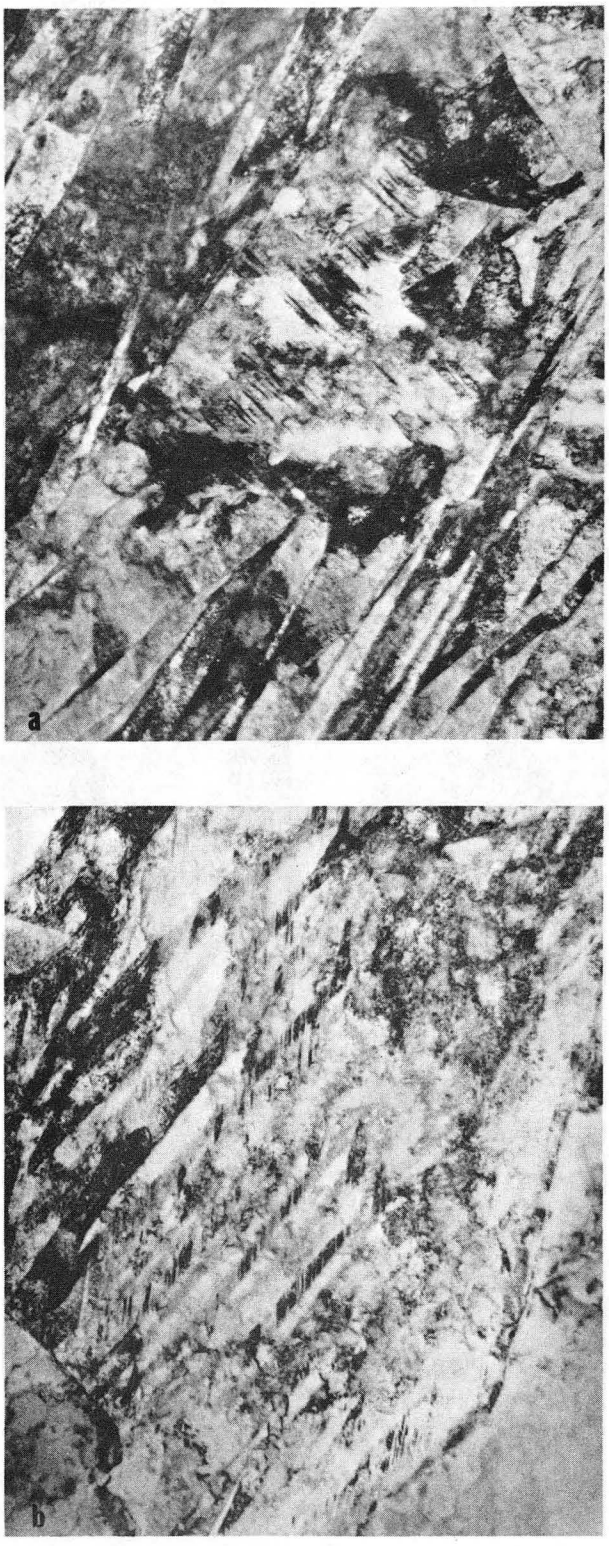

XBB 751-752

Fig. 9

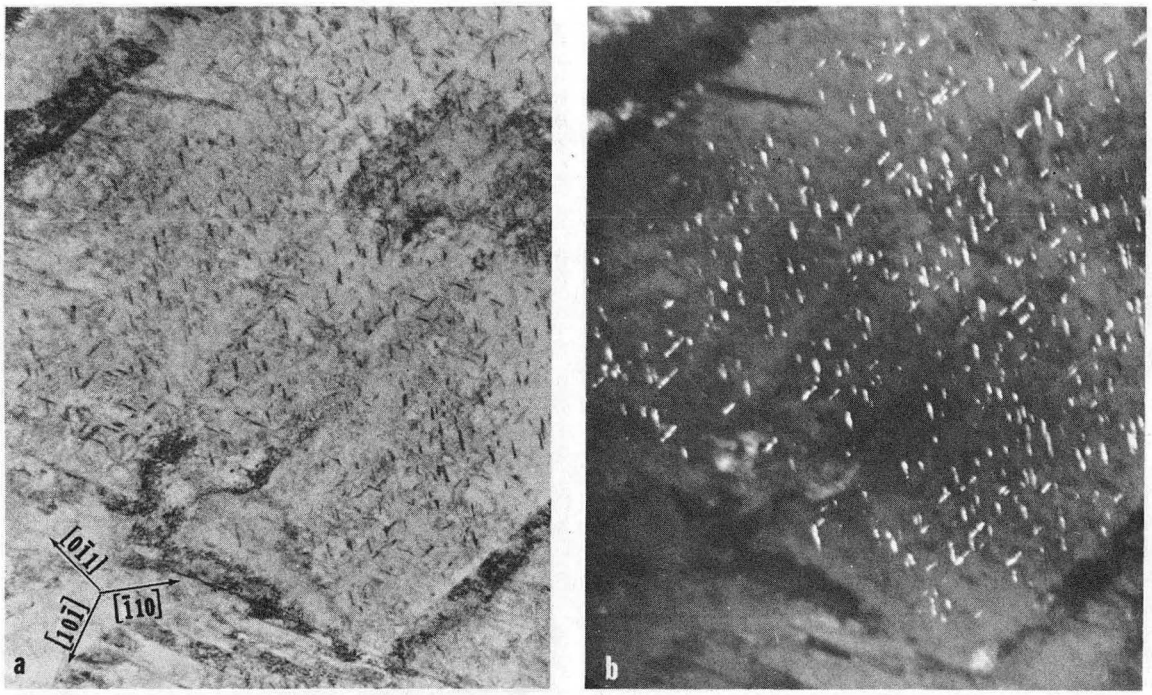

XBB 751-753

Fig. 10

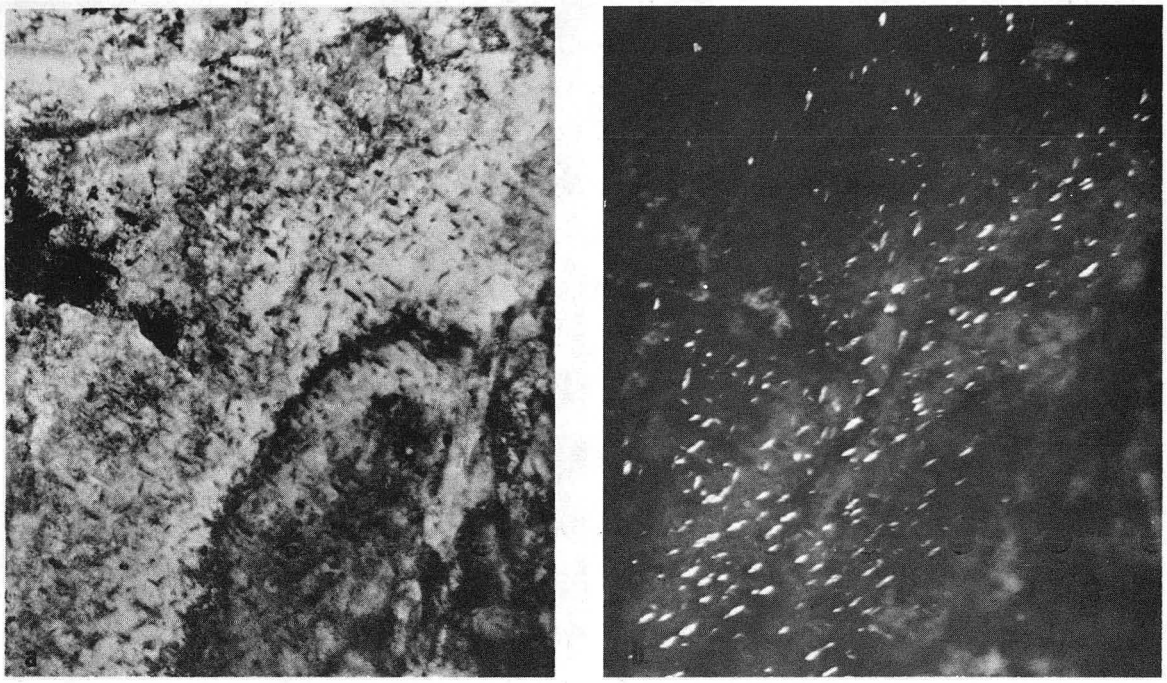

XBB 751-754

Fig. 11

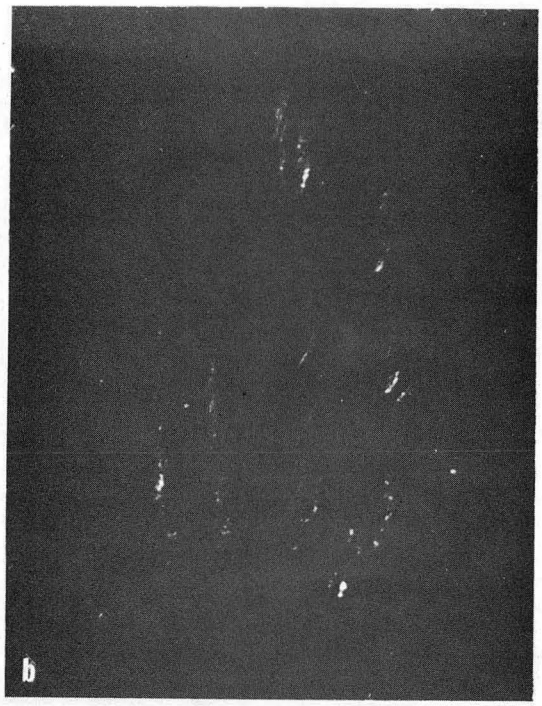

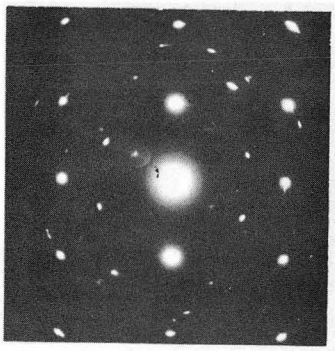

c

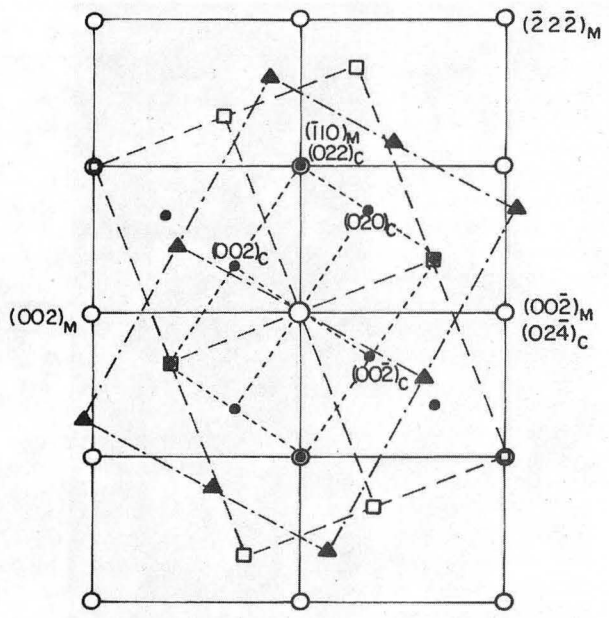

d

○ <110> Martensite Orientation

• [100] Cementite Orientation

□ ▲ } Other <110> Martensite Orientations

XBB 751-766

Fig. 12

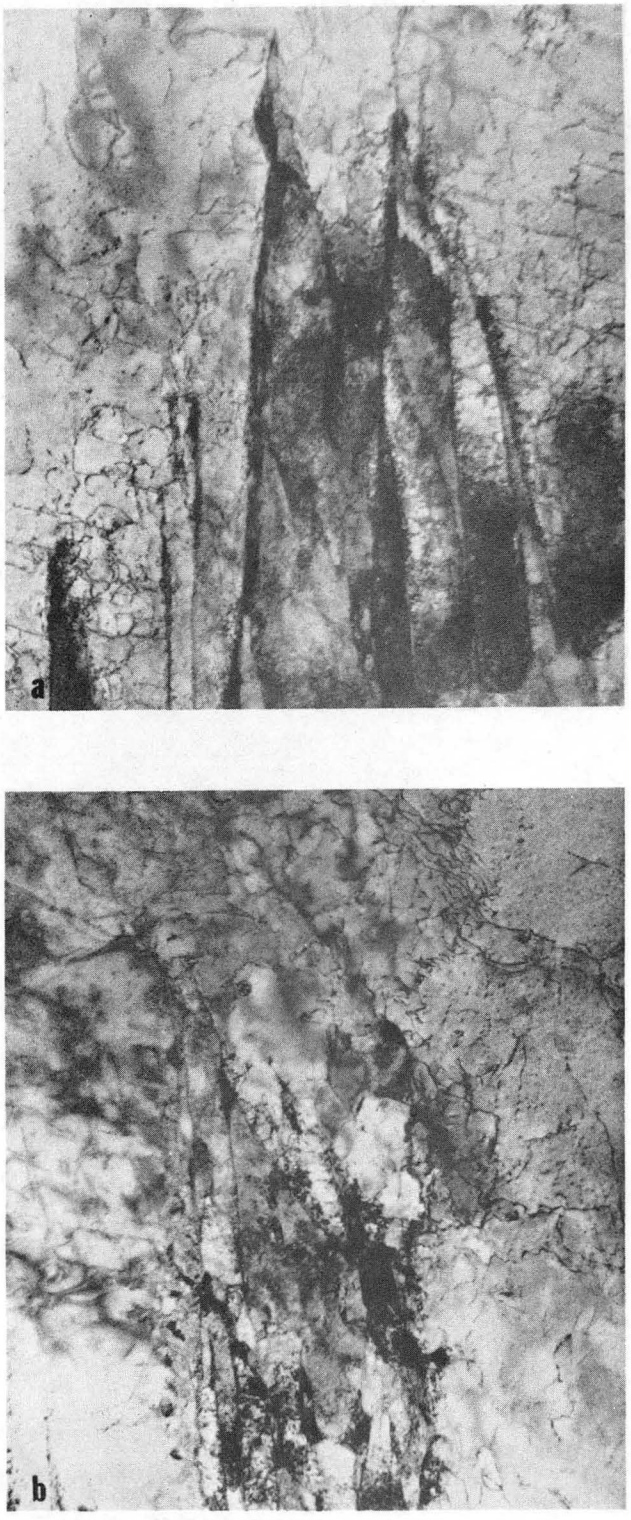

XBB 751-842

Fig. 13

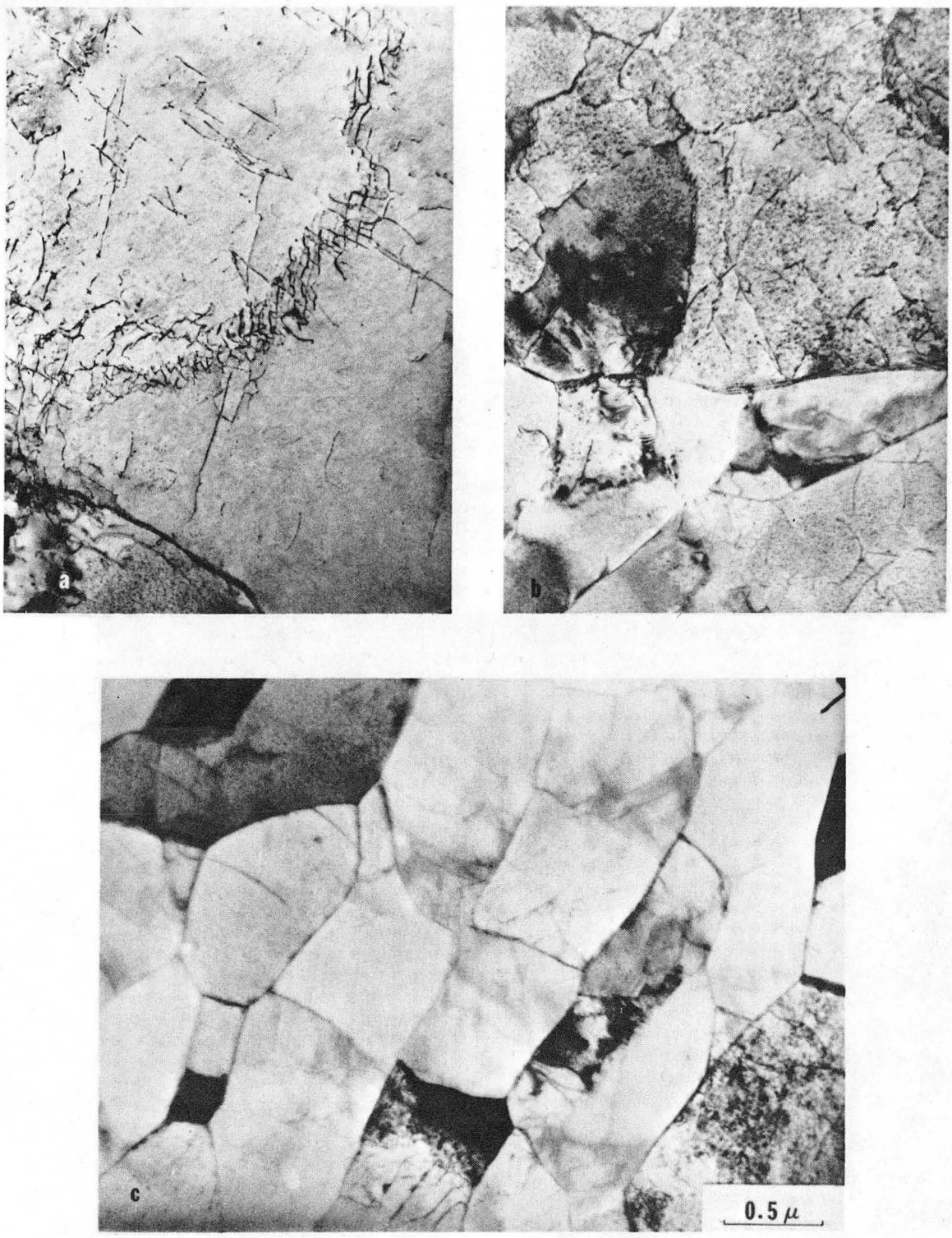

XBB 751-758

Fig. 14

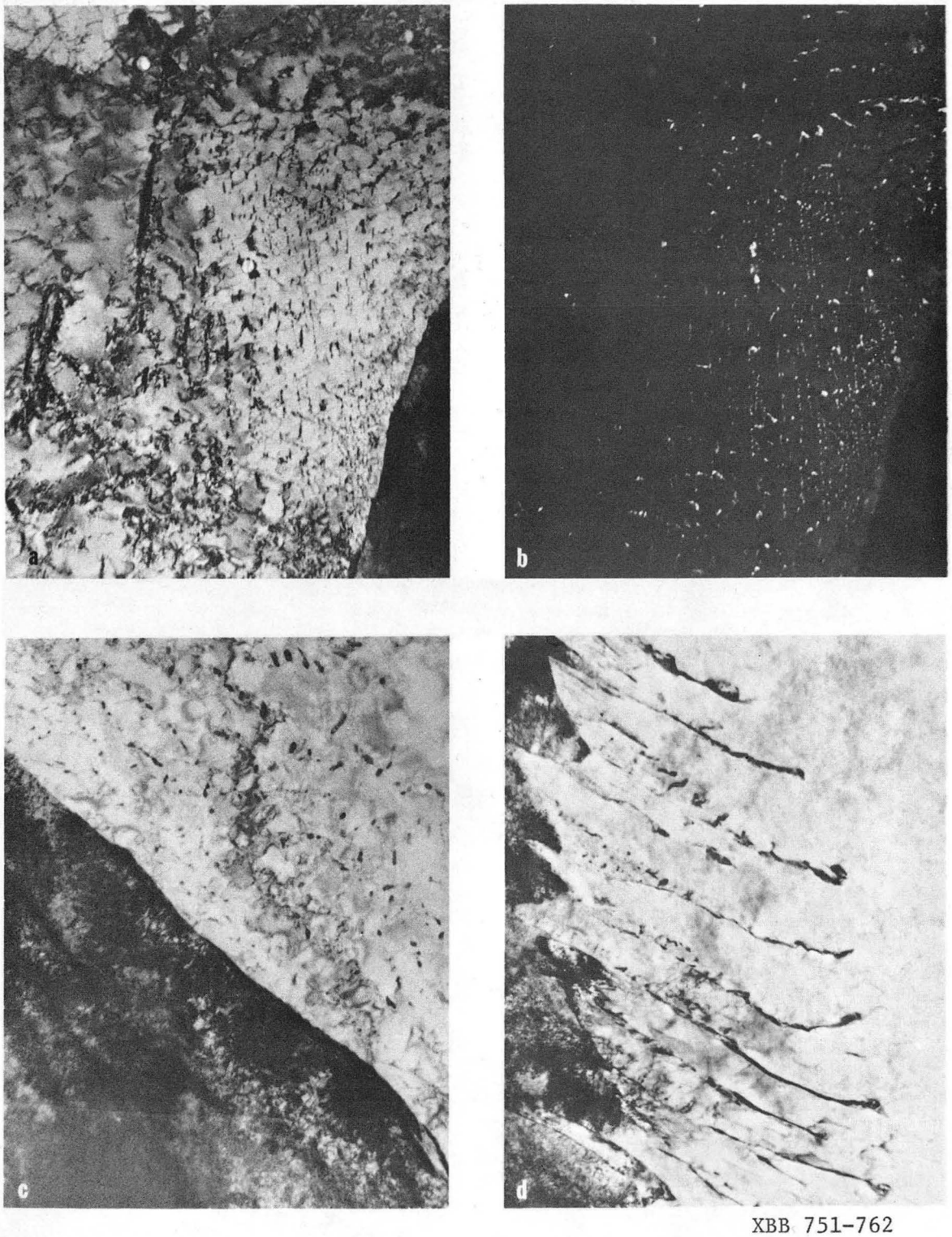

XBB 751-762

Fig. 15

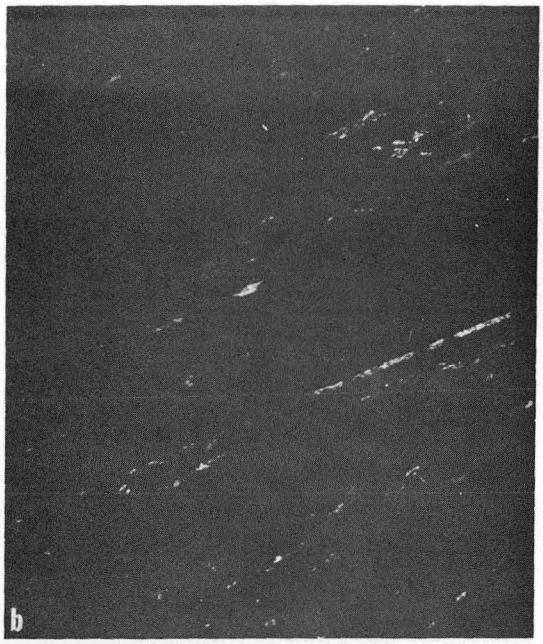

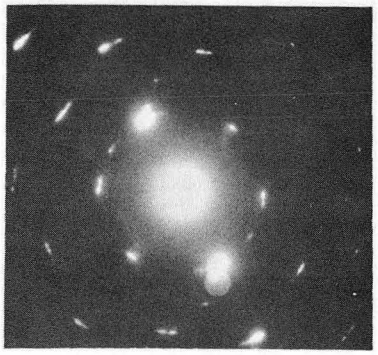

c

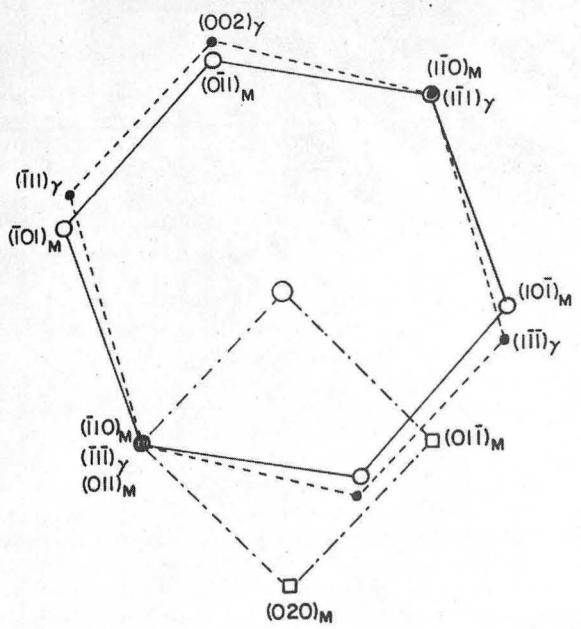

d

XBB 751-765

Fig. 16

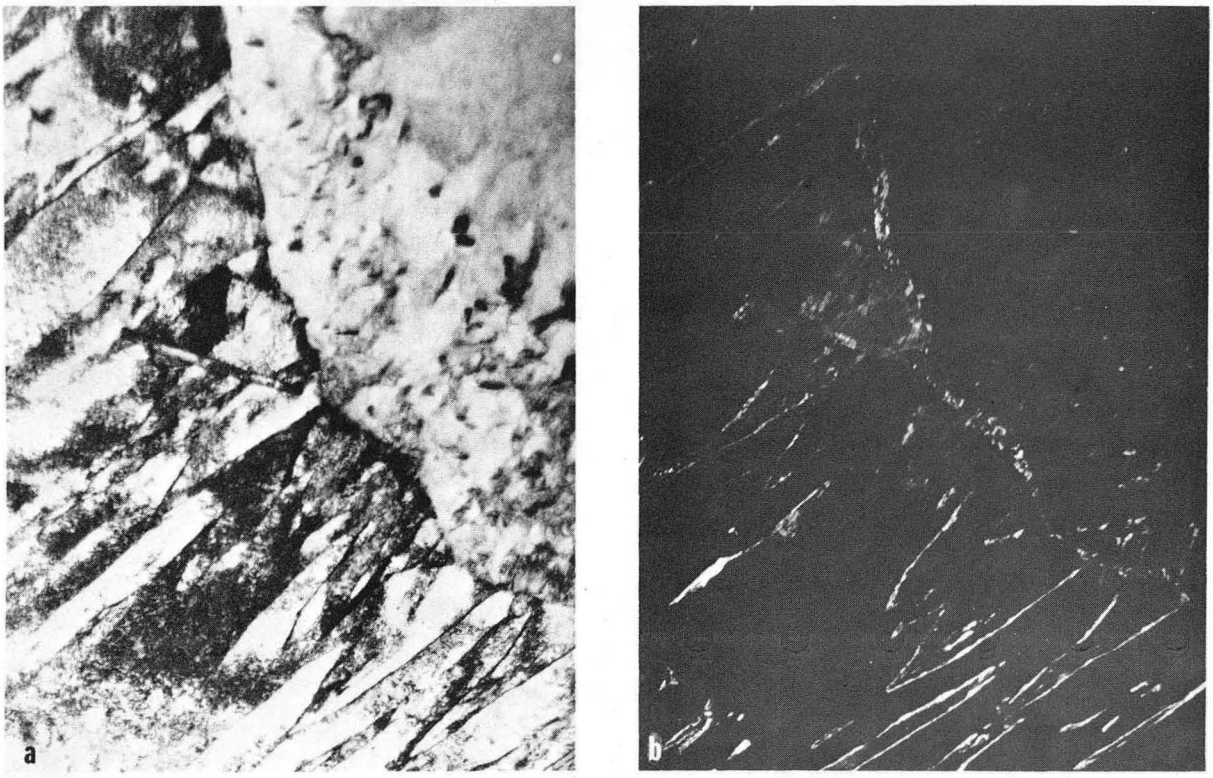

XBB 751-755

Fig. 17

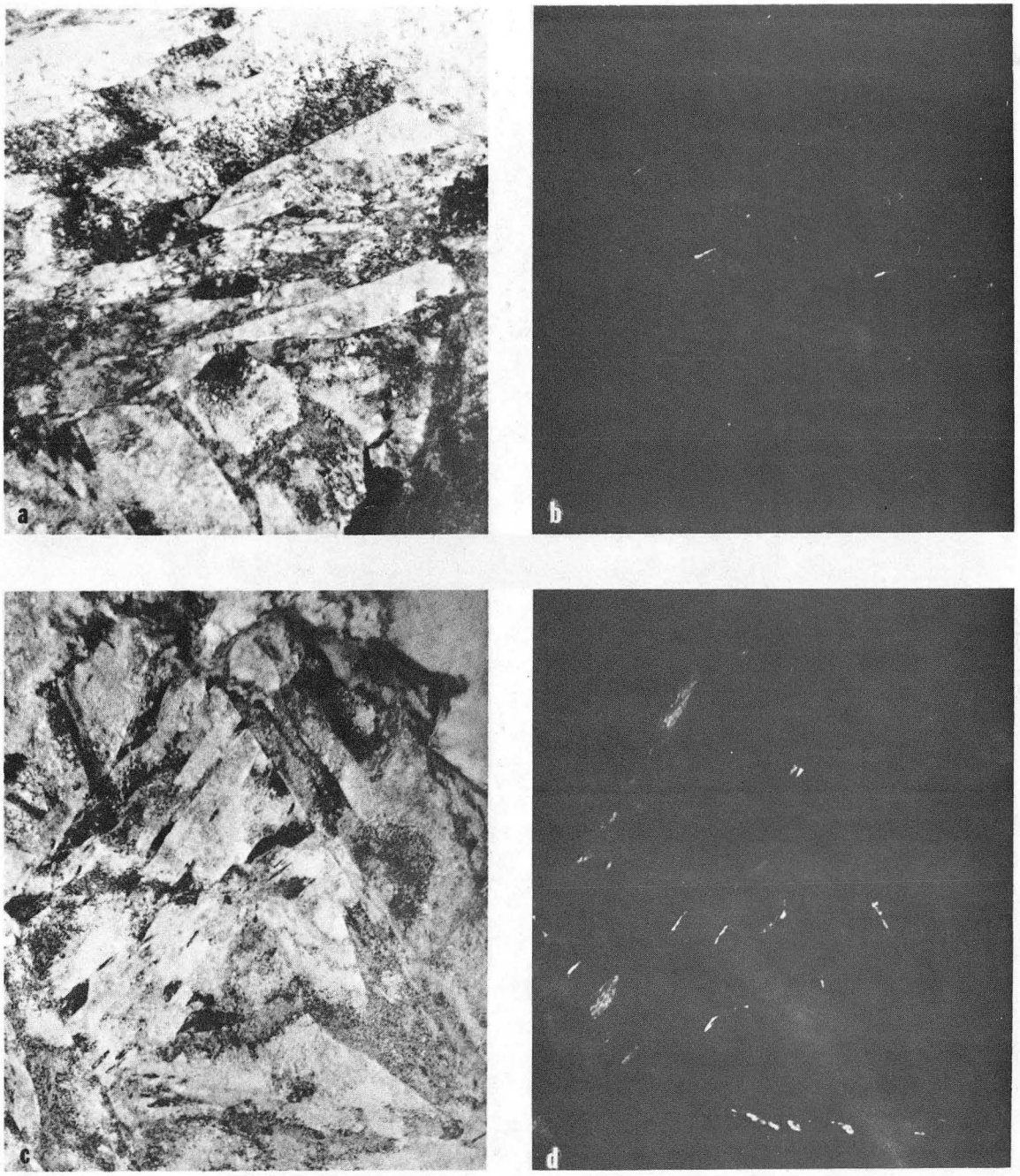

XBB 751-761

Fig. 18

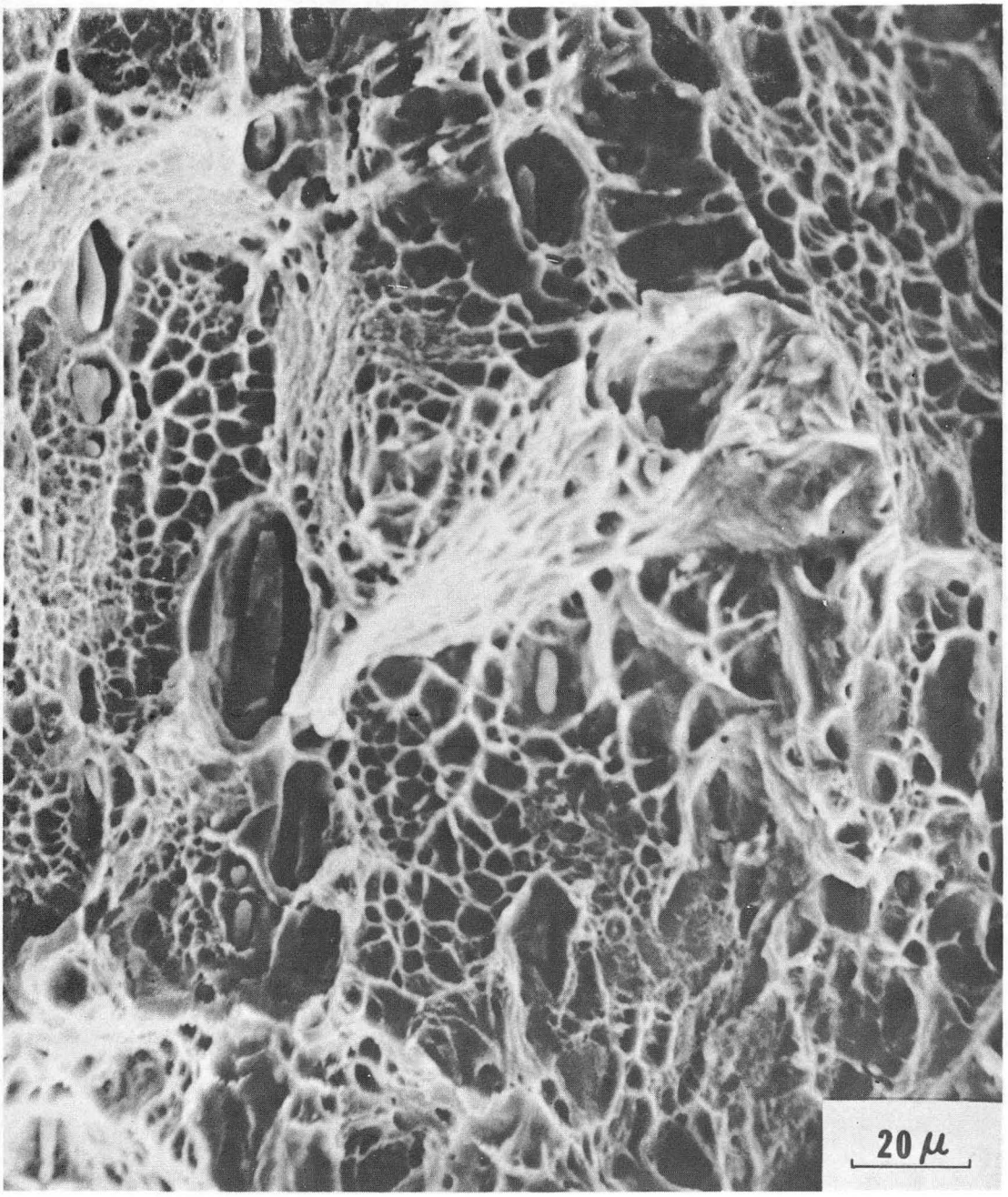

XBB 751-764

Fig. 19

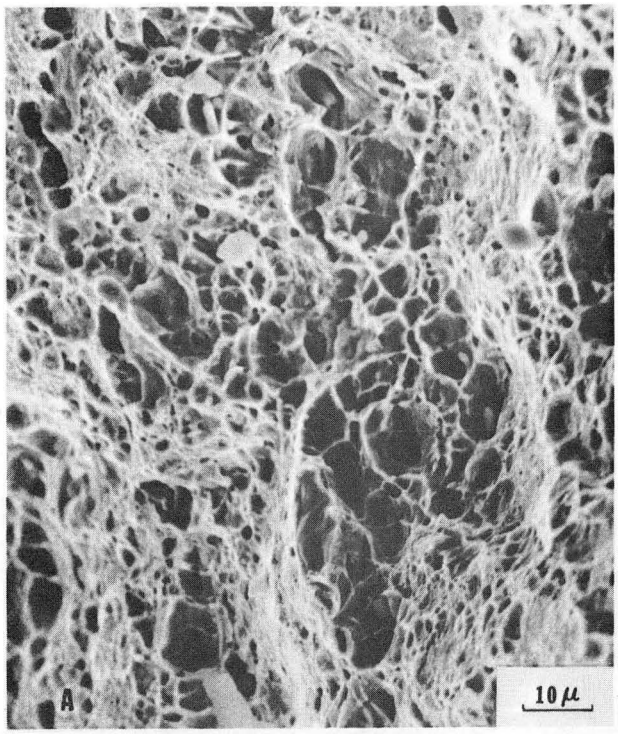

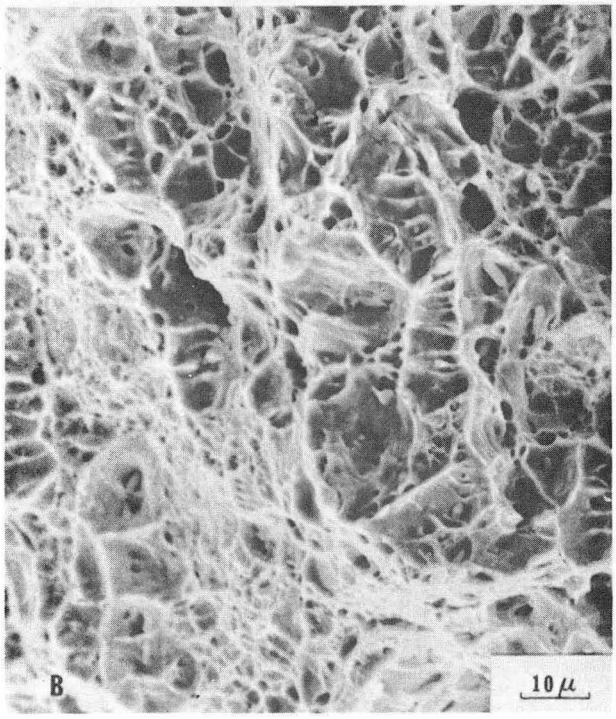

XBB 751-841

Fig. 20

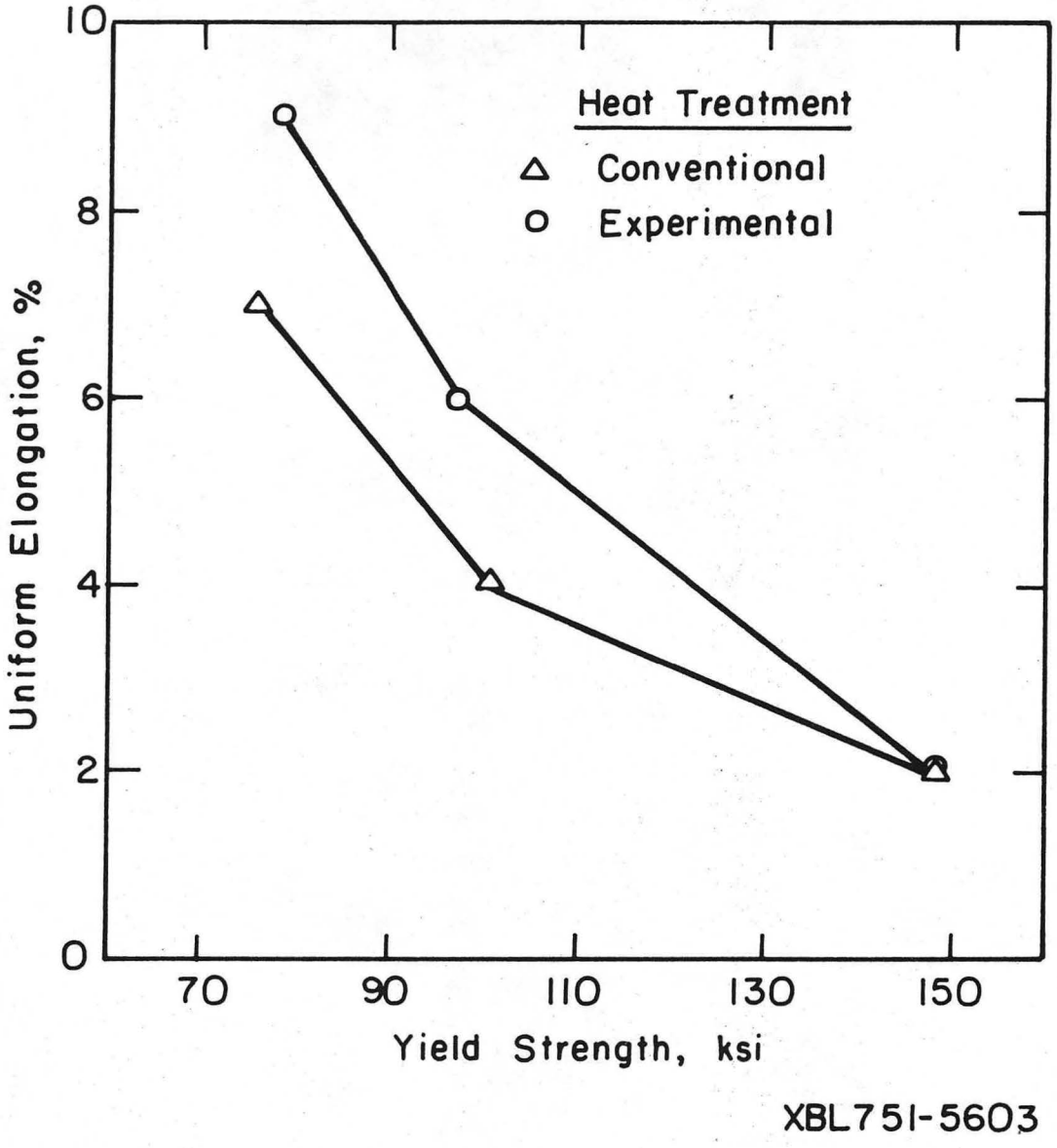
Heat Treatment
Conventional
Experimental
Uniform Elongation, %
Yield Strength, ksi
0
2
4
6
8
10
70
90
110
130
150
XBL751-5603

Fig. 21

TECHNICAL INFORMATION DIVISION
LAWRENCE BERKELEY LABORATORY
UNIVERSITY OF CALIFORNIA
BERKELEY, CALIFORNIA 94720